

# BULLETIN

DE LA SOCIÉTÉ DES SCIENCES ET DES LETTRES DE ŁÓDŹ

2018

Vol. LXVIII

---

Recherches sur les déformations

no. 1

---

pp. 33–54

*Stanisław Bednarek and Julian Płoszajski*

## A COIL GENERATING HIGH AND HOMOGENOUS MAGNETIC FIELDS

### Summary

This paper deals with an innovative design of a coil producing magnetic fields up to the magnitude of 55 T within a volume of approximately a few dm<sup>3</sup>. The initial part of the paper describes of the design of the coil. The effective magnetic field in the coil is produced in a cylindrical volume located eccentrically inside a cylinder. Winding of the coil consisted of wires parallel to the cylinder and axes which protrude out of the device. The coil wires have been made of tungsten and cooled with liquid helium. The next part of the paper included calculations concerning the spatial distribution of the magnetic field induction. Approximate calculations were conducted for an infinitely long coil and precise calculations for a coil of limited length. Basic parameters for the power supply and cooling systems were also calculated. The collected results were compared with present technical possibilities and the feasibility of the project was discussed. Significant features of the coil include the high uniformity of the magnetic field produced, reduction of the dispersed field outside the coil as well as its low thermal power loss.

*Keywords and phrases:* coil, cylinder, volume, magnetic field, uniformity, tungsten, cooling, liquid helium

### 1. Introduction

High and constant magnetic fields have many important applications, including among others in scientific research, modern technologies and medical diagnostics [1, 2]. Generation of such fields require the use of coils made of resistive conductors or superconductors which are cylindrical in shape. Wires in those coils form concentric circles or rings. The latter variant appears in so-called Bitter magnets [3, 4]. The effective magnetic field is generated inside a cylindrical space, the axis of which is directed through the center of the scroll. Disadvantages of this solution, include

among other things: a decrease of the magnetic field induction when distance from the center of the opening increases and the appearance of a highly dispersed field outside the coil.

This paper shows a design of the coil for which the effective magnetic field is generated within a cylindrical space with a of radius  $r_1$  which is located inside a cylinder with a radius equal  $r_2$ . The cross-section of the device is shown schematically in Fig. 1. Axis of the cylinder 1 and the axis of the recess 2, are parallel but offset with regard to one another by distance  $d$ . It has been shown that if a current of density  $j$  flows in parallel to its axis of such a recess, through a long cylinder, then a uniform magnetic field is produced within such a recess. The initial assumption is that the length of the cylinder  $l$  is much greater than its radius, which means that the conditions  $l \gg r_1, r_2, d$  are met. The magnetic field induction  $B_c$  at any point A inside the recess is calculated using the Superposition and Ampere's Laws [5]. In such case, the recess 2 is replaced with a cylinder, in which the electric current flows in a direction opposite to that as in cylinder 1. The resultant total current within the recess equals 0 which corresponds to the real situation. Using the designations accepted at Fig. 1, the magnetic field induction produced by a section of the cylinder and by the recess at point A, labelled respectively as  $\mathbf{B}_1$  and  $\mathbf{B}_2$  are expressed by the formulas

$$\mathbf{B}_1 = \frac{\mu_0 (\mathbf{j} \times \mathbf{a})}{2}, \quad (1)$$

$$\mathbf{B}_2 = \frac{\mu_0 (\mathbf{j} \times \mathbf{b})}{2}, \quad (2)$$

where  $\mu_0$  represents the magnetic permeability of a vacuum. Moreover, for vectors  $\mathbf{a}$  and  $\mathbf{b}$  indicating the position of point A, it is true that

$$\mathbf{d} = \mathbf{a} - \mathbf{b}. \quad (3)$$

Using the superposition principle and formulas (1–3), it follows that

$$\mathbf{B}_c = \mathbf{B}_1 + \mathbf{B}_2 = \frac{\mu_0 (\mathbf{j} \times \mathbf{d})}{2} = \text{const.} \quad (4)$$

The formula (4) shows that the value of magnetic field induction is constant and directly proportional to the current density as well as the distance between the axes of the recess and of the cylinder. It is due to this, that in order to increase the magnetic field induction, the recess must be located as far as possible from the axis of the cylinder. It would be best if the recess were adjacent to the cylinder surface and have a relatively low radius. Fulfillment of the second condition does however result in limitation of effective recess volume in which the effective magnetic field is produced.

The results collected are true for an infinitely long cylinder as Ampere's law is in such case, fulfilled completely. In practice, a monolithic cylinder with a recess could be substituted by a bundle of parallel wires filling up the space between the

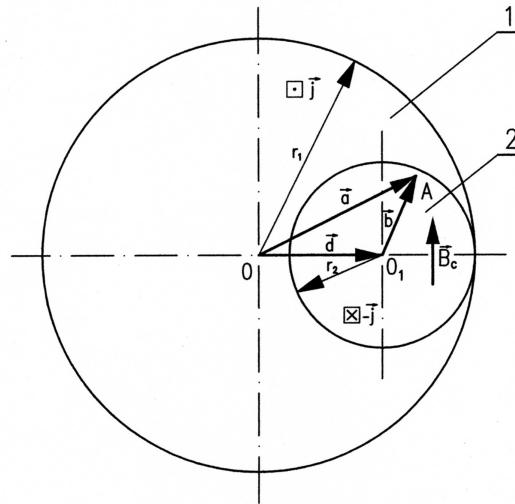


Fig. 1. Outline for magnetic field induction calculations inside a cylindrically shaped recess inside the conductor; 1 – conductor, 2 – recess,  $\mathbf{j}$  – current density,  $\mathbf{B}_c$  – inductivity inside the recess ( $\mathbf{B}_c = \text{const.}$ ),  $r_1$  – conductor radius,  $r_2$  – recess radius,  $d$  – distance between the cylinder and recess axes.

cylinder surface and outer recess surface. This concept along with the property of a magnetic field, have been used within the coil proposed. Moreover, the cylinder with the recess were located in a coaxial cylinder which is filled up by a bundle wires. The wire bundle is composed of the same number of wires but the current inside them would flow in the opposite direction. As a result, the magnetic field outside the entire device has been reduced while the cylinder did not generate a magnetic field inside the recess.

## 2. Coil design

The details of the coil design have been shown in Fig. 2 [6]. Inside the insulating pipe 1 is a cylindrical working chamber 2 which is separated by a partition 3 and is tangent to the pipe. The pipe 1 has been located coaxially at the cylinder shell consisting of two halves 4, 5, covered from inside with insulation and bound together by screws 6. The insulated wire which was used to made the coil winding passes in parallel to its axis, filling the entire space inside as well as outside the pipe. Each winding of the coil is made straight-line sections 7, 8, passing respectively inside and outside of the pipe and arched sections 9, 10, located behind the ends of the pipe. The wire and the shell contain holes designed to transport cooling liquid to the winding. These holes overlap and create pass-through ducts 11. The quantities of wire sections 7, 8, which are located inside and outside of the insulated pipe 1 are equal.

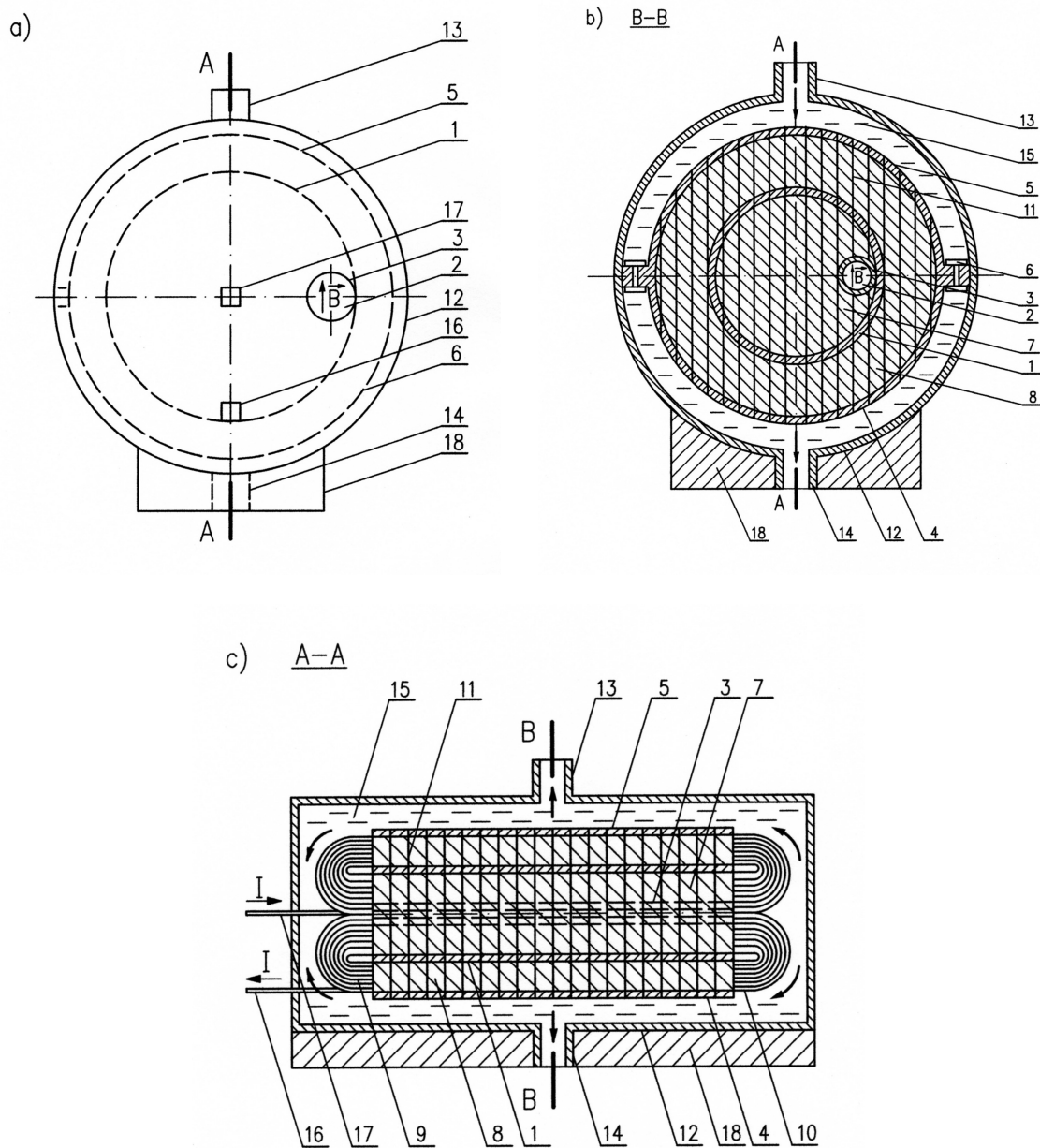


Fig. 2. Coil design: a) view from one end, b) transversal cross-section, c) longitudinal section, 1 – insulating pipe, 2 – recess (operating chamber), 3 – recess wall, 4, 5 – halves of the shell, 6 – bolt, 7 – straight-line section of wire inside the pipe, 9, 10 – arched wire sections, 11 – cooling channel, 12 – thermos-insulating cover (Dewar vessel), 13 – inlet pipe, 14 – exit pipe, 15 – cooling fluid, 16, 17 – wire ends, 18 – base.

As a result, the surfaces of the transversal cross-sections, contained between inner wall of the pipe and outer wall of the recess 3 and between the half shells 4, 5, must be equal. The coil is enclosed in a heat insulating casing 12 (a Dewar vessel with double partitions), provided with an inlet and outlet pipes 14 that are designed to

provide cooling liquid flow 15. The ends of the coils 16, 17 are led out of the housing 12 and connected to a direct current power source. The coil and its housing are placed horizontally on the base 18.

The housing halve 4, 5 which have been bound together by screws 6, protect the coil against being torn apart by electro-dynamic forces directed radially outside. These forces appear because of current flow in opposite directions through the straight-line sections of the wire 7, 8 located inside and outside of the insulator pipe 1. The half shells 4, 5, the screws 6, the cover 12 and the base 18 should be made of non-ferromagnetic materials characterize by a high mechanical durability such as austenitic steel. For the purposes of decreasing the thermal loss, the winding will be cooled down to cryogenic temperature. The most appropriate material for the production of the winding is tungsten which doesn't reach the state of superconductivity but has at the temperature of several Kelvin degrees, a very low resistivity of a magnitude of approximately  $10^{-12} - 10^{-13} \Omega\text{m}$ . Cryogenic temperatures are possible to reach by means of cooling with the use of liquid helium. Because tungsten is at these temperatures still in a resistive state, the problem of exceeding the critical field doesn't exist. This problem does occur in area of superconductors. It occurs when the intensity of flowing current becomes high enough that it exceeds the critical field which causes a rapid growth in the electrical resistance. A superconductor passes into the resistive state. Moreover, tungsten is characterized by a very high mechanical durability. This is a very positive feature as coils assigned to produce high magnetic fields are subjected to very strong tensions caused by the electrodynamic forces. The material tetrafluoroethylene (also known as Teflon) may be applied as an insulating material of high mechanical durability, suitable to work in low temperature we may also be applied.

### 3. Spatial distribution of the magnetic field induction for a long coil

The basic meaning of the spatial distribution of the magnetic field induction produced by the coil has practical applications, especially the as part of the calculation of values of induction within the operative recess. Firstly, we apply the assumption that the length of the coil is much greater than its radius and other the transversal dimensions ( $l \gg r_1, r_2, d$ ), which is referred to as the infinitely long cylinder model. The crosssection of such a cylinder with appropriate notations was shown in Fig. 3a. Keeping with above assumptions it is possible to calculate numerical values of the induction outside  $B_0$  and inside  $B_i$  of the cylinder by applying well known formulas resulting from the Ampere's Law [5, 7].

$$B_0 = \frac{\mu_0 I}{2\pi r}, \quad (5)$$

$$B_i = \frac{\mu_0 j r}{2r}. \quad (6)$$

The  $I$  within the formulas [5, 6] represents the total current intensity flowing through the cylinder,  $j$  – the effective current density, while  $r$  – the distance of the point at which the field induction is calculated from the cylinder axis. The assumption made earlier that the areas of transversal cross-sections, contained between inner insulating wall of pipe 1 and the external wall of the recess 3 as well as the between external wall of the pipe and the inner wall of the half-shell 4, 5 are equal (Fig. 2b). The assumptions have allowed to formulate the formula:

$$S_h = \pi (r_2^2 - r_1^2) = \pi (r_4^2 - r_3^2), \quad (7)$$

from which we may calculate the coil's outside radius  $r_4$

$$r_4 = \sqrt{r_2^2 + r_3^2 - r_1^2}. \quad (8)$$

Because the wire is covered with insulation, the effective current density is lower than the current density inside the wire  $j_1$ . If the wire were to have a square side cross-section including insulation, marked as  $g$  while thickness of insulation marked as  $g_1$ , then the following condition is fulfilled

$$I = j_1 (g - 2gt_1)^2 = jg^2. \quad (9)$$

Formula (9) allows for calculations of the effective current density  $j$ , as an average density in the transversal cross-section of the wire. We thereby obtain

$$j = j_1 \left( \frac{g - 2g_1}{g} \right)^2. \quad (10)$$

An application of a wire with a square cross-section makes it easier to fill the space inside and outside the insulating pipe 1 and increases effective current density (Fig. 2). Moreover such side-by-side arrangement of wires with a square cross-section, makes easier making to form canals for cooling fluid. Let  $B_1$ ,  $B_3$ ,  $B_2$  represent components of the magnetic field induction coming from inner and external parts of winding and the recess respectively. Let  $B_w$ ,  $B_c$  mean the net induction and the induction inside the recess (effective induction) respectively. Then, using formulas (5, 6) the superposition principle and condition (7) a set of formulas has been formulated which allows to calculate magnetic field induction at the transversal cross-section depending on the distance from coil axis  $r$ . It has assumed that the recess is a cylinder with a radius  $r_2$ , through which flows a current with a density labelled as  $j$ .

The derived formulas have been collected in Tab. 1. Fig. 3b. shows qualitative charts of each magnetic field induction derived by the application of those formulas. It was further assumed that dimensions of the coil possible to practical realization will be:  $r_1 = 0.05$  m,  $r_2 = 0.5$  m,  $d = 0.45$  m,  $r_3 = 0.51$  m. For these values, it has been calculated from formula (8) that  $r_4 = 0.71$  m. Current density inside the wire  $j_1 = 250$  A/m<sup>2</sup>, thickness of the wire with insulation  $g = 10$  mm and a thickness

of the insulation  $g_1 = 1$  mm have all been assumed. The effective current density was calculated using formula (10) and yielded the value of  $j_1 = 250$  A/mm<sup>2</sup>. The assumed current density is approximately 25 times greater than the current density applied in commonly used electrical installations made of copper. Those installations are however not cooled. If wires are cooled, then the current density can be much higher. In the case of internal coils of a Bitter magnet which are intensely cooled with water, the current density reach up to 600 A/mm<sup>2</sup> [1]. Therefore, the current density accepted for the calculation has been well founded. Using formulas listed in Tab.1. and the accepted values, the components of magnetic field induction have been calculated while their graphs have been presented in Fig. 4. It follows from them that the magnetic field induction inside of the recess would allow to reach the value of  $B_c = 56.6$  T.

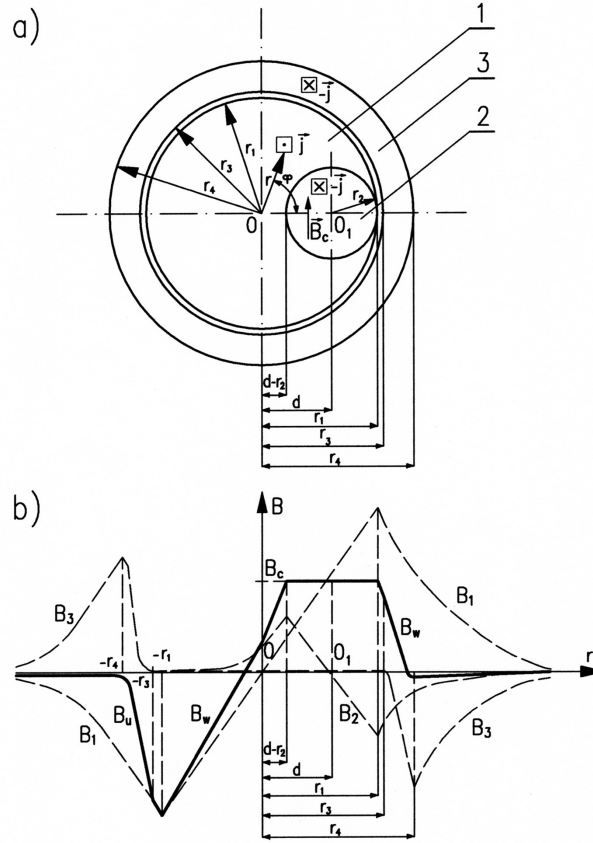


Fig. 3. Outline of magnetic field induction calculations as a transversal cross-section for the infinitely long coil (a) and changes of field  $B$  along distance from the coil axis  $r$  (b); 1 – inner part of the coil winding, 2 – recess, 3 – external part of coil winding,  $\mathbf{j}$  – current density,  $\mathbf{B}_w$  – resultant field induction,  $\mathbf{B}_c$  – resultant field induction inside the recess ( $\mathbf{B}_c = \text{const.}$ ),  $r_1, r_2, r_3, r_4$  the radii of: the inner axis of winding, the recess, external insulating pipe, external part of winding,  $d$  – the distance of recess axis from the winding axis.  $B_1, B_2, B_3$ .

Table 1. Arrangement of formulas used in calculations of magnetic field induction;  $j$  – current intensity,  $r_1, r_2, r_3, r_4$  – radii respectively of: inner part of the winding, recess, external insulating pipe, external winding part,  $d$  – distance of recess axis from winding axis,  $B_1, B_2, B_3$  – components of magnetic field induction appropriately coming from: inner and external parts of the winding,  $B_w, B_c$  – induction respectively of: the resultant and within the recess (effective).

Lp.	Współrzędna $r$ względem osi (opis obszaru)	Składowe indukcji $B_1, B_2, B_3$	Indukcja wypadkowa $B_w = B_1 + B_2 + B_3$
1.	$-r_1 < r < d - r_2$ (w wewnętrznej części uzwojenia poza wnęką)	$B_1 = \frac{\mu_o jr}{2}$ $B_2 = -\frac{\mu_o jr_2^2}{2(r-d)}$ $B_3 = 0$	$B_w = \frac{\mu_o j}{2} \left[ r - \frac{r_2^2}{r-d} \right]$
2.	$d - r_2 < r < r_1$ (we wnęce)	$B_1 = \frac{\mu_o jr}{2}$ $B_2 = -\frac{\mu_o j(r-d)}{2}$ $B_3 = 0$	$B_1 = \frac{\mu_o jd}{2} = const$ ( $B_w = B_c$ )
3.	$r_1 < r < r_3$ $-r_4 < r < -r_3$ (wewnątrz izolacji)	$B_1 = \frac{\mu_o jr_1^2}{2r}$ $B_2 = -\frac{\mu_o jr_2^2}{2(r-d)}$ $B_3 = 0$	$B_w = \frac{\mu_o j}{2} \left[ \frac{r_1^2}{r} - \frac{r_2^2}{r-d} \right]$
4.	$r_3 < r < r_4$ $-r_4 < r < -r_3$ (w zewnętrznej części uzwojenia)	$B_1 = \frac{\mu_o jr_1^2}{2r}$ $B_2 = -\frac{\mu_o jr_2^2}{2(r-d)}$ $B_3 = -\frac{\mu_o j(r^2 - r_3^2)}{2r}$	$B_w = \frac{\mu_o j}{2} \left[ \frac{r_1^2}{r} - \frac{r_2^2}{r-d} - r \right]$
5.	$r < -r_4$ $r > r_4$ (na zewnątrz cewki)	$B_1 = \frac{\mu_o jr_1^2}{2r}$ $B_2 = -\frac{\mu_o jr_2^2}{2(r-d)}$ $B_3 = -\frac{\mu_o j(r_4^2 - r_3^2)}{2r}$	$B_w = -\frac{\mu_o j}{2} \left[ \frac{r_2^2 d}{r(r-d)} \right]$

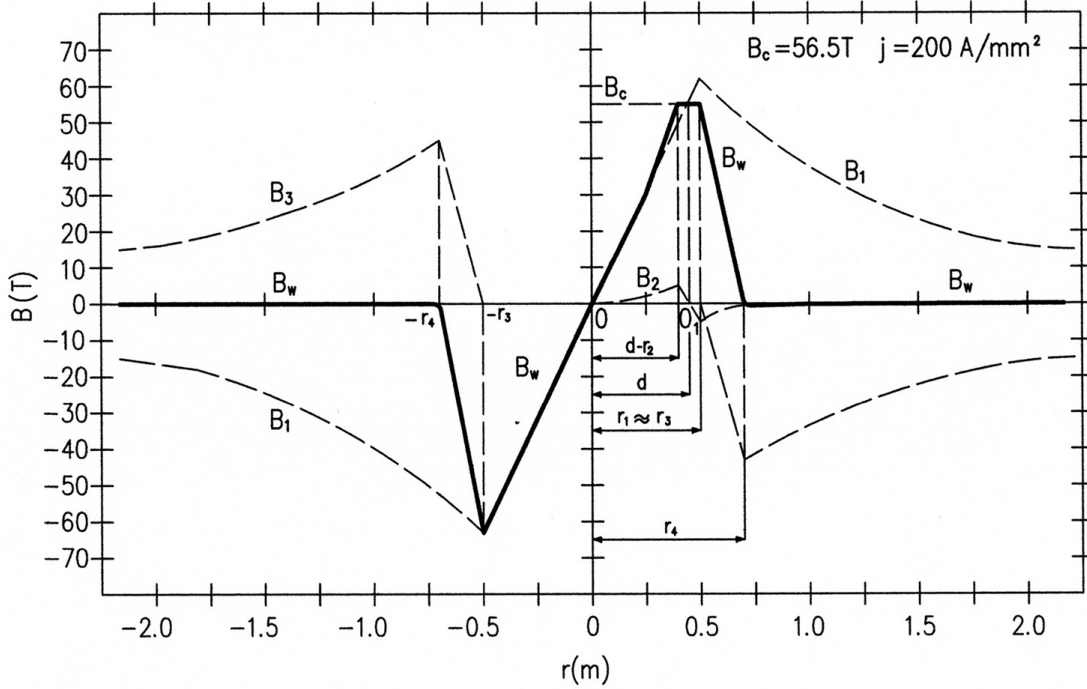


Fig. 4. The chart of magnetic field induction  $B$  as a function of distance from infinitely long coil axis for current density  $j = 200 \text{ A/mm}^2$ ,  $B_1$ ,  $B_2$ ,  $B_3$  – components of magnetic field induction resulting respectively from: inner and external parts of winding and recess,  $B_w$ ,  $B_c$  – respective induction of: the net and within the recess (effective).

#### 4. Spatial distribution of coil field induction of limited length

It is obvious that a feasible coil must have a limited length which would in practice be comparable with its diameter. It is for this reason that more precise calculations must be performed for this case. In order to simplify the calculations, an initial condition was accepted as with a narrow straight-line conductor of limited length  $l$  which conducts a current with an intensity of  $dl$  (Fig. 5). The contribution  $dB$  to the magnetic field induction, as generated by the conductor at point P, located at the distance  $u$  from the conductor as measured along a line perpendicular to it and located at the distance  $z$  from its end ( $0 \leq z \leq l$ ) has been by formula [8]

$$dB = \frac{\mu_0 dl}{4\pi u} (\sin \alpha_1 + \sin \alpha_2). \quad (11)$$

Sins of the angles  $\alpha_1$ ,  $\alpha_2$  in formula (11) are calculated by the formulas

$$\sin \alpha_1 = \frac{z}{\sqrt{u^2 + z^2}}, \quad (12)$$

$$\sin \alpha_2 = \frac{l - z}{\sqrt{u^2 + (l - z)^2}}. \quad (13)$$



coil axis. Using the cosine theorem for an OPA triangle and designations assumed in Fig. 6 it is possible to calculate  $u$

$$u = \sqrt{r_p^2 + r^2 - 2rr_p \cos \varphi}. \quad (14)$$

Using the polar frame of reference  $r, \varphi$ , the current intensity  $dI$  inside the conductor is expressed by means of the formula

$$dI = j dS = jr d\varphi dr. \quad (15)$$

The polar angle  $\varphi$  appearing in formula (15) fulfils the condition  $0 \leq \varphi \leq 2\pi$ . The contribution  $dB$  to the magnetic field induction is decomposed into the radial component  $dB_r$  and the tangent component  $dB_t$ , the numerical values of which are expressed by formulas

$$dB_r = dB \cos \beta, \quad (16)$$

$$dB_t = dB \sin \beta. \quad (17)$$

For the OPA triangle, the sinus theorem may be used which is represented by the formula

$$\frac{u}{\sin \varphi} = \frac{r}{\sin(90^\circ - \beta)} = \frac{r}{\cos \beta}. \quad (18)$$

Using formula (18) we get the following expressions for the trigonometric functions as represented in formulas (16), (17).

$$\cos \beta = \frac{r}{u} \sin \varphi, \quad (19)$$

$$\sin \beta = \sqrt{1 - \left(\frac{r}{u} \sin \varphi\right)^2}. \quad (20)$$

After substitution of formulas (11), (15) and subsequently (19), (20) into the formulas (16), (17), the following expressions are obtained for component contributions  $dB_r, dB_t$  of the magnetic field induction at point P:

$$dB_r = \frac{\mu_0 j}{4\pi} (\sin \alpha_1 + \sin \alpha_2) \left(\frac{r}{u}\right)^2 \sin \varphi dr d\varphi, \quad (21)$$

$$dB_t = \frac{\mu_0 j}{4\pi} (\sin \alpha_1 + \sin \alpha_2) \left(\frac{r}{u}\right) \sqrt{1 - \left(\frac{r}{u} \sin \varphi\right)^2} dr d\varphi. \quad (22)$$

In order to calculate magnetic field induction values produced by a cylinder with a length  $l$ , the inner radius  $r_w$  and outer radius  $r_z$  at chosen point P at the coordinates  $z, r_p$ , the following double integrals may be calculated:

$$B_r(z, r_p) = \frac{\mu_0 j}{4\pi} \int_{r=r_w}^{r=r_z} \int_{\varphi=0}^{\varphi=2\pi} (\sin \alpha_1 + \sin \alpha_2) \left(\frac{r}{u}\right)^2 \sin \varphi dr d\varphi, \quad (23)$$

$$B_r(z, r_p) = \frac{\mu_0 j}{4\pi} \int_{r=r_w}^{r=r_z} \int_{\varphi=0}^{\varphi=2\pi} (\sin \alpha_1 + \sin \alpha_2) \left(\frac{r}{u}\right) \sqrt{1 - \left(\frac{r}{u} \sin \varphi\right)^2} dr d\varphi, \quad (24)$$

in which  $u$ ,  $\sin \alpha_1$ ,  $\sin \alpha_2$  are expressed by the respective formulas (12), (13) and (11). It is easy to notice that because of the periodicity of the sine function, the result of calculation of (23) limited by  $0 \leq \varphi \leq 2\pi$  gives a value of 0. As a result, the magnetic field has only the component  $B_t$  and is therefore directed perpendicularly to the surface passing through the cylinder axis.

In order to calculate the spatial distribution of the net magnetic field induction, produced by the coil in question, formula (24) was applied at first to calculate components coming from separate elements of the winding, like in the case of the earlier analyzed infinitely long coil. In formula (24) limits of integration were chosen appropriately to the radii of elements  $r_1, r_2, r_3$  and  $r_4$ . Next, the superposition rule was used to calculate spatial distribution of the net magnetic field induction. For purposes of the calculations, the length of cylindrical parts of the coil was assumed to be  $l = 2$  m along with the earlier given values of their radii and current density. The conducted calculations omitted the influences resultant from arched parts of wires 9, 10, which are outside the insulating pipe 1 because the current flow directions are directly opposite resulting in their near mutual compensation. The obtained spatial distributions of magnetic field induction  $B$  produced by the individual coil elements are shown in Fig. 7–9 while Fig. 10 presents the spatial distribution of the resultant magnetic field induction produced by the coil. In turn, Fig. 11–13 showed dependencies of the net magnetic field induction  $B_w$  from distance of the coil axis  $r$  at its transverse plane symmetry, passing respectively: through its transverse plane symmetry, in the middle point of the coil's length and through the very end of coil. Fig. 14 showed the variability of the net magnetic field induction  $B_w$  along recess axis.

As was foreseeable, the magnetic field induction produced by the coil of limited length  $l = 2$  m is less than the approximate one obtained from a long coil. The maximal induction at the middle of the coil recess is  $B_{\text{cmax}} = 55.1$  T (a result of 55.6 T was obtained for the infinitely long coil). As results, from the analysis of charts at Fig. 4 and Fig. 11–12, we see that difference for the assumed coil length and a long one is rather small. The net magnetic field induction of a limited length coil decreases along with the distance from the middle of recess  $z$  measured along its axis. Changes for those distances  $z < 0.25 l$  are relatively small and equal to approximately

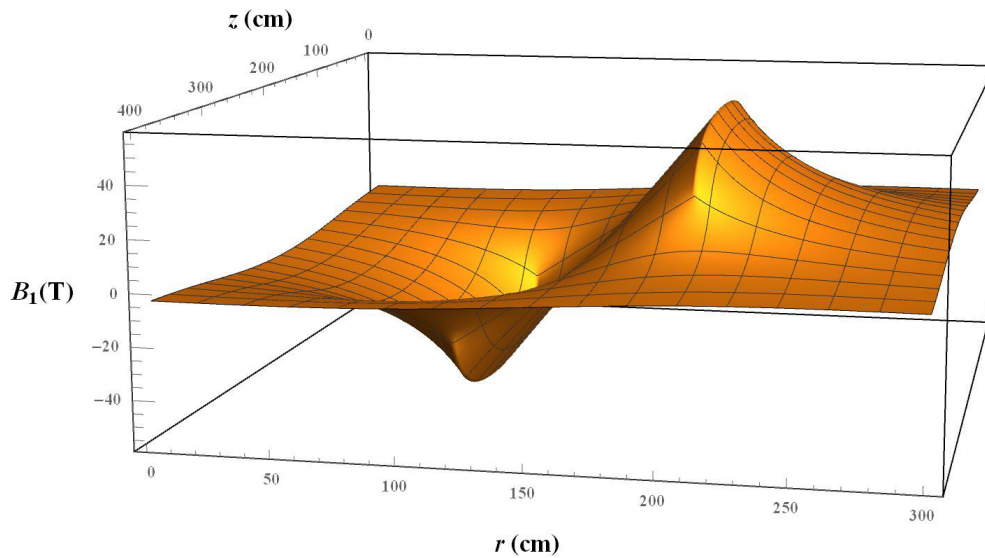


Fig. 7. Spatial distribution of magnetic field induction  $B_1$ , produced by the inner part of winding – full cylinder of radius  $r_1 = 0.5$  m and length  $l = 2$  m, by the effective current density  $j = 200$  A/mm<sup>2</sup>, the middle of the cylinder is at the point of coordinates  $r = 150$  cm and  $z = 200$  cm.

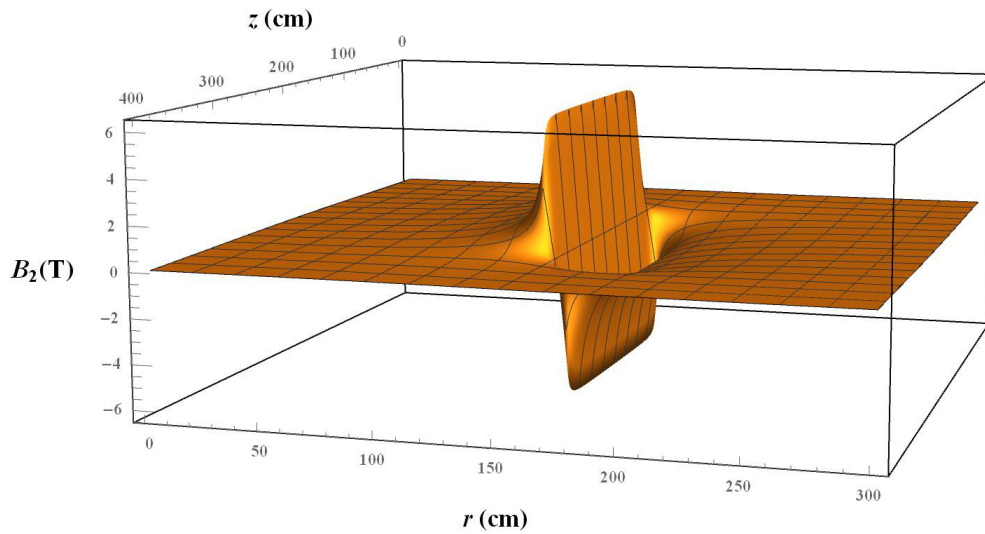


Fig. 8. Spatial distribution of magnetic field induction  $B_2$ , produced by the recess – full cylinder of radius  $r_1 = 0.05$  m and length  $l = 2$  m, by the effective current density  $j = 200$  A/mm<sup>2</sup>, cylinder axis passes at distance  $d = 0.45$  m from the coil axis, and its middle is located at the point of coordinates  $r = 195$  cm and  $z = 200$  cm.

2.5 T. We observe a significant drop of the net magnetic field induction at the end of the coil, where induction drops down to 28 T. Moreover, as seen in Fig. 11–12 changes of the net magnetic field induction inside the recess due to an increase of distance  $r$  from the coil axis in its transverse plane symmetry and at transverse cross-section plane in the middle of the coil length, are practically not noticeable.

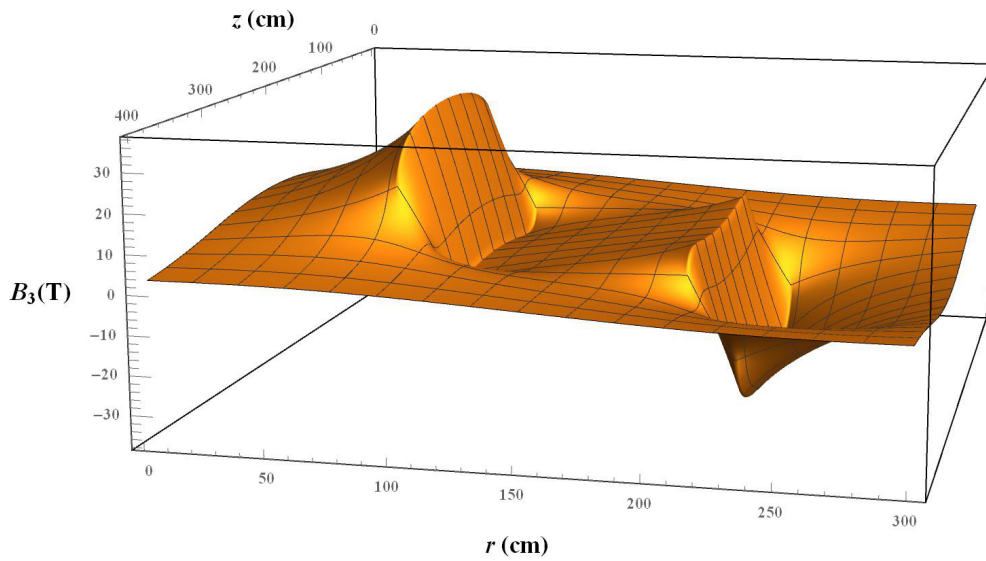


Fig. 9. Spatial distribution of magnetic field induction  $B_3$ , produced by the external part of winding – pipe with radii: internal  $r_1 = 0.51$  m, external  $r_2 = 0.71$  m and length  $l = 2$  m, by effective current density  $j = 200$  A/mm<sup>2</sup>, the middle of pipe is located at the point of coordinates  $r = 150$  cm and  $z = 200$  cm.

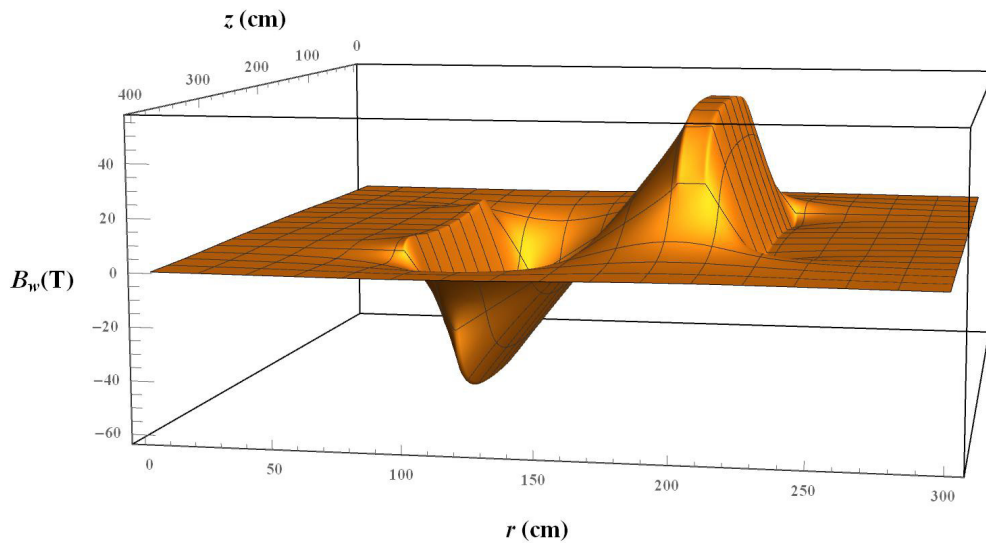


Fig. 10. Spatial distribution of the net magnetic field induction  $B_w$ , produced by the coil consisting of elements shown in Fig. 7–9 (superposition of charts Fig. 7–9) the middle of the coil is located at the point of coordinates  $r = 150$  cm and  $z = 200$  cm.

A significant advantage of the considered coil is that despite its large value of the useful magnetic field induction inside of recess and a large field volume, the magnetic field induction outside of the coil, a so-called dispersed field, is relatively small. The chart shown in Fig. 14 shows that at a distance of 0.5 m from the ends of the coil, the dispersed field induction is equal to approximately 3 T. The charts found in Fig. 11–13 do however show that for the same distance from the coil's side

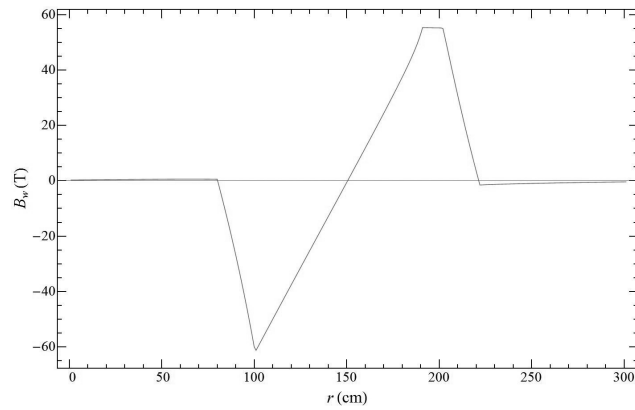


Fig. 11. Dependence of the net magnetic field induction  $B_w$  from the distance of coil axis  $r$  at its transverse plane symmetry ( $z = 200$  cm).

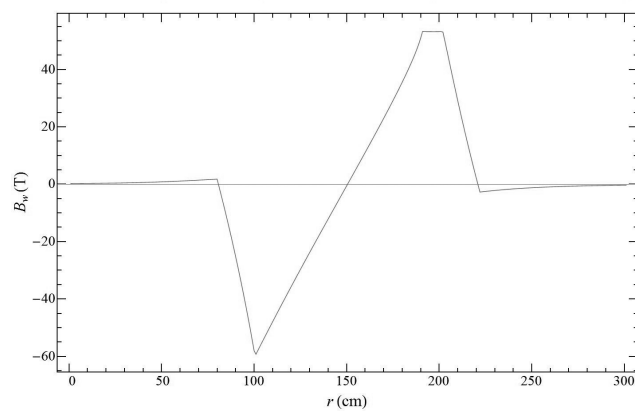


Fig. 12. Dependence of the net magnetic field induction  $B_w$  from distance of coil axis  $r$  at transverse plane symmetry passing at the distance  $z = \pm 0.25l$  (150 cm or 250 cm) measured along the recess axis.

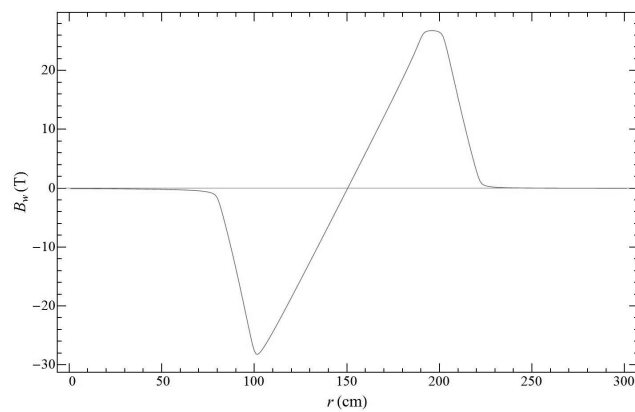


Fig. 13. Dependence of the net magnetic field induction  $B_w$  from distance of coil axis  $r$  at transverse plane symmetry passing through the end of the coil  $z = \pm 0.5l$  (100 cm or 300 cm).

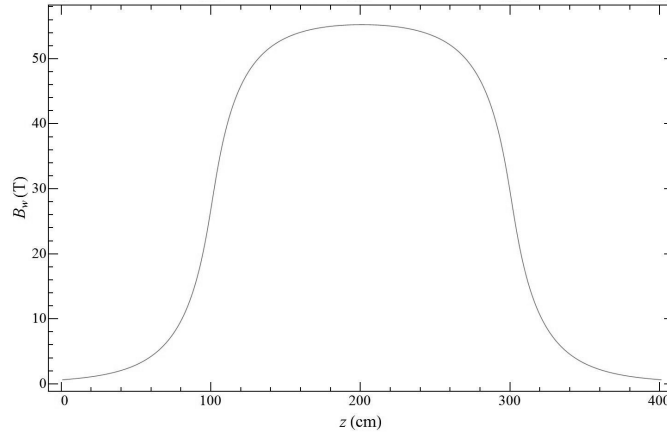


Fig. 14. Dependence of the net magnetic field induction  $B_w$  from distance  $z$  measured along recess axis  $r = d$  (195 cm).

surface, the field induction is negligibly small. The dispersed field induction could be even lower after taking into account into calculations the arched parts of wires 9, 10 (Fig. 2c). The current inside these parts flows in opposite directions and decreases the dispersed field induction.

## 5. Parameters of the power supply system

Of paramount importance to the estimation of the feasibility of the coil are calculations of the parameters of its power supply. Because the coil works in a resistive state, the power supply requires delivery of power  $P$  as expressed by the formula

$$P = \Delta UI, \quad (25)$$

where  $I$  represents the intensity of the current flowing through the winding and  $\Delta U$  symbolizes the drop of voltage. The wire has a square cross-section of side  $g$  and an effective current density inside it is  $j$  and therefore the total current intensity is calculated using the formula

$$I = jg^2. \quad (26)$$

Effective current density was calculated from formula (10) and equaled 200 A/mm<sup>2</sup>. Because of side of the wire equals  $g = 10$  mm, the total current intensity  $I = 20$  kA. In accordance with Ohm's Law, the voltage drop on the winding is

$$\Delta U = IR_p, \quad (27)$$

where  $R_p$  represents the total resistance of the wire used for the winding. The total resistance may be calculated from the formula

$$R_p = \frac{\rho l_p}{g^2}, \quad (28)$$

where  $l_p$  signifies the total length of wire,  $\rho$  – the resistivity of the material used. In order to calculate  $l_p$  the number of windings forming the coil should be known. Because the winding totally fulfills space between insulating pipe 1 and the recess wall 3, it is possible to state that

$$n_p = \frac{\pi (r_1^2 - r_2^2)}{g^2}. \quad (29)$$

After entering the earlier-obtained dimensions from formula (29) we get  $n_p = 7770$ . Each scroll is made of two straight-line sections of wire with a length  $l$  with one feeding inside and the second one outside insulating pipe  $l$  and with two arcs connecting those sections around the end of the pipe. For simplicity it has been assumed that each arc is  $\Delta l$  long so the total length of wire is express by the formula

$$l_p = 2(l + \Delta l)n_p. \quad (30)$$

For the coil dimensions assumed the value of  $\Delta l = 0.5$  m was accepted. The winding should be composed of tungsten and cooled by liquid helium. Assuming the temperature of the winding to be 1 K, where the resistivity of tungsten was  $\rho = 1.6 \cdot 10^{-13} \Omega\text{m}$  [9]. After entering this value and the earlier accepted coil dimensions into formula (30) and (28) the value  $R_p = 1.6 \cdot 10^{-5} \Omega$  was obtained. The calculated result  $R_p$  was substituted into formula (27) and receiving thereby the voltage drop to be  $\Delta U = 1.57$  V. Finally, the power supply was calculated to be  $P = 30$  kW. Because winding operates in resistive state, this power is dissipated in the form of heat. If no cooling system were present, the coil temperature would increase leading to an increase in the electrical resistance as well. This could in turn lead to the increase of dissipated heat quantity, causing an overheating which could destroy the insulation of the coil.

## 6. Cooling system parameters

Keeping of the resistivity assumed for tungsten requires a heat collection system. It is for this reason very important to secure an effective cooling system of winding. In order to evaluate the feasibility of this undertaking, the basic parameters of the cooling system were calculated. The heat collection in systems cooled by liquid helium is realized by the evaporation of the liquid [10, 11]. The evaporation heat of liquid helium at a temperature of 1 K equals  $c_p = 1.5 \cdot 10^{-4}$  J/kg. Therefore, the mass of helium  $m_h$  which should flow during 1 s in order to remove the power  $P$  (so called flow intensity) is expressed by the formula

$$m_h = \frac{P}{c_p}, \quad (31)$$

while the volume  $V_h$  of liquid helium is expressed as

$$V_h = \frac{m}{\rho_h}, \quad (32)$$

where  $\rho_h = 145 \text{ kg/m}^3$  is density of helium. After substitution of appropriate values into formulas (31), (32) we get  $m_h = 2.28 \text{ kg/s}$  and  $V_h = 15.7 \text{ dm}^3/\text{s}$ . Evaporating liquid helium increases its volume  $k_e$  times. This number is called the factor of expansion and is equal to  $k_e = 746$ , so volume of gaseous helium is expressed by the formula

$$V_g = V_h k_e. \quad (33)$$

From formula (33) we obtain  $V_g = 11.8 \text{ m}^3/\text{s}$ . Assuming appropriate diameters of cooling channels, it was possible to calculate velocity  $v$  of helium flow rate and the related differences of pressure  $\Delta p$ . Assuming the average channel diameter is equal  $d_k = 3.6 \text{ mm}$  and the total number of channels is  $n_k = 2 \cdot 10^4$ . The area of a transversal cross-section of a single channel  $S_{k1}$  may be calculated using the formula

$$S_{k1} = \frac{\pi d_k^2}{4} \quad (34)$$

and is equal to  $S_{k1} = 10 \text{ mm}^2$ . If we mark the total area of all channels as  $S_k$  than flow velocity can be calculated using the formula

$$v = \frac{V_g}{n_k S_{k1}}. \quad (35)$$

After substitution we obtain  $v = 56 \text{ m/s}$ . For comparison, the total area of all channels was  $S_k = 0.2 \text{ m}^2$  which was approximately 7.1% of the area of an axial cross-section of the coil in question, having a total area equal to  $2.8 \text{ m}^2$ . For verification if calculated flow was laminar Reynold's number  $R_e$  was calculated using the formula

$$R_e = \frac{\rho_{gh} d_k v}{\eta}, \quad (36)$$

where  $\rho_{gh} = 0.164 \text{ kg/m}^3$  represents the density of gaseous helium, while  $\eta$  – its viscosity. After substitution into the formula (36)  $\rho_{gh} = 0.164 \text{ kg/m}^3$  and  $\eta = 0.0149 \text{ Pa}\cdot\text{s}$  we got  $R_e = 2219$ . Because critical value of Reynold's number is 2300, it showed that the flow was laminar. Therefore we could calculate the pressure difference  $\Delta p$  using Hagen-Poiseuille formula due to according to which  $\eta = 0.0149 \text{ Pa}\cdot\text{s}$

$$\Delta p = \frac{8\pi\eta v V_{hg}}{n_k S_{k1}^2}. \quad (37)$$

After substituting appropriate values into formula (37) we got  $\Delta p = 1.2 \cdot 10^3 \text{ Pa}$  which corresponded to 0.023 ATM. This value is not very large and achieving it does not pose any technological challenges.

## 7. Mechanical durability of windings

A significant problem was posed by the mechanical tensions observed inside coils which produced the high magnetic fields. In commonly used cylindrical coils, these compression stresses compress along their axes while they stretch along the radial direction. These stresses are caused by interaction of coil elements in which currents flow in same or opposite directions [12]. In the coil under consideration, compression stresses appear between winding sections located inside the insulating pipe 1 and stretching stresses acting upon sections located outside the pipe (Fig. 2a). It is for this reason that a shell was designed, consisting of two halves 4, 5, which, when fastened together with bolts 6, transfers some of these stretching stresses and increasing thereby the durability of the coil (Fig. 2b). Value of those stresses  $\sigma$  is equal to density of the magnetic field at a given point of the coil and can be calculated with the formula

$$\sigma = \frac{B^2}{2\mu_0}. \quad (38)$$

In accordance with Fig. 4, the maximum value of the induction calculated in approximate way for a long coil was equal to 60 T. For such an induction we obtained  $\sigma = 1.43 \cdot 10^9 \text{ N/m}^2$  using formula (38) while durability against stretching tungsten as  $\sigma_r = 1.72 \cdot 10^9 \text{ N/m}^2$ . It can be concluded that the stretching durability of the coil will not be exceeded. The provided durability of  $\sigma_r$  is valid for room temperatures while the durability in cryogenic conditions is greater [10]. This would mean that the coil in question using with tungsten windings has a certain reserve in terms of its durability. After transformation of formula (38) it was possible to calculate that exceeding the given tensile strength for tungsten would occur in a magnetic field with an induction of  $B = 65.7 \text{ T}$ .

## 8. Conclusions

The results collected indicated that the maximal value of magnetic field induction  $B_{\text{cmax}} = 55.1 \text{ T}$  generated by the coil in question is approximately 20 T bigger than the induction produced by the most powerful resistive Bitter magnets [13]. This induction is comparable with field induction produced by hybrid magnets, consisting of Bitter magnets located inside large dimension superconducting magnet cooled by liquid helium. The tensile strength of windings made of tungsten is not exceeded even in the fields generated. For the coil dimensions assumed, an effective magnetic field obtained for testing, is several tens of times larger in volume than in large Bitter magnets. This does however mean that the dimensions of such a coil are several times greater than of those magnets.

Power necessary to supply the coil in the magnitude of approximately 30 kW is very low in comparison with power delivered to Bitter magnets producing fields of

magnetic induction of 30 T. This represents approximately  $10^{-3}$  of power supplying those magnets [14]. Current intensity of the power supply  $I = 20$  kA has a comparable value as in the case of Bitter magnets. The flow intensity of liquid helium necessary to keep a steady temperature of the windings, despite its heat dispersion, also has a similar value as in the case of high magnetic field producing systems equipped with cryogenic cooling [15].

The comparisons conducted allow for the assumption of the hypothesis that the coil design considered here could constitute a useful source of high and steady magnetic fields of induction comparable to those generated by hybrid magnets. The advantage of such a coil would include: high homogeneity of effective field and its large volume combined with a reduced dispersed field outside of the winding. Verifying those hypotheses requires further research, the object of which would include solving detailed technical problems, such as the way of connecting winding sections or creation of the cooling channels. An interesting topic of future research could include calculation of what values of magnetic induction may be achieved in presently used Bitter magnets with of plate sets made of tungsten and cooled by liquid helium, similarly to the coil considered here. Another important question is what power would need to be supplied in order to produce magnetic field with an induction matching presently in those magnets while using plates made of cooper and being cooled by water.

## References

- [1] [1] H. J. Schneider-Muntau (Editor), *High magnetic fields: Applications, generations, materials*, World Scientific, Singapore, New Jersey, London, Hong Kong 1997, 9.
- [2] J. C. Xia, C. Vicente, E. D. Aoms, N. S. Sullivan, *The National High Magnetic Field Laboratory Ultra-High B/T Facility*, Physica B **346–347** (2004), 649–653.
- [3] M. Motokawa, K. Watanabe, S. Awaji, *High magnetic field research in Tohoku University*, Current Applied Physics **3** (2003), 367–376.
- [4] K. Trojnar, N. Koppetzki, *High Field Magnets at the International Laboratory Wroclaw*, Physica B **155** (1989), 85–86.
- [5] J. Griffiths, *Introduction to Electrodynamics*, Prentice Hall Inc., Upper Saddle River, New Jersey (1981), 181.
- [6] S. Bednarek, *Cewka do wytwarzania silnych jednorodnych pl magnetycznych*, opis zgłoszeniowy wynalazku do Urzędu Patentowego RP nr 420617 (2017).
- [7] H. Rawa, *Elektryczność i magnetyzm w technice*, Wydawnictwo Naukowe PWN, Warszawa 1994, 283.
- [8] E. M. Purcell, *Electricity and Magnetism, Berkeley Physics Course*, Vol. 2, MacGraw-Hill Book Company, New York 1965, 239.
- [9] W. Mizerski, *Tablice fizyczno-astronomiczne*, Wydawnictwo Adamantan, Warszawa 2013, 173.

- [10] K. Mendelson, *Cryogenics*, Wiley and Sons, Inc., New York 1950, 85.
- [11] B. Truck, *Tore supra: A tokamak with superconducting toroidal field coils*, IEEE Transactions on Magnetism **25** (1989), 1473–1480.
- [12] M. Motokawa, H. Nojiri, Y. Tokunaga, *An idea for the easy construction of a high field magnet*, Physica B **155** (1989), 96–99.
- [13] F. Herlach, *Magnets*; in: Encyclopedia of Applied Physics, Vol. 9, VCH Publishers Inc., New York 1994, 254.
- [14] J. F. Herlach, N. Miura, *High Magnetic Fields Science and Technology, Vol. 1 Magnet Technology and Experimental Technique*, World Scientific, New Jersey, London, Singapore, Shanghai, Hong-Kong, Taipei, Bangalore 2003, 125.
- [15] G. B. Lubkin, *Florida dedicated National High Magnetic Field Laboratory*, Physics Today **12** (1994), 21–23.

Chair of Informatics  
University of Łódź  
Pomorska 149/153, PL-90-236 Łódź  
Poland  
E-mail: bedastan@uni.lodz.pl  
julian-p@wp.pl

Presented by Leszek Wojtczak at the Session of the Mathematical-Physical Commission of the Łódź Society of Sciences and Arts on June 22, 2017.

## CEWKA DO WYTWARZANIA SILNYCH JEDNORODNYCH PÓL MAGNETYCZNYCH

### S t r e s z c z e n i e

Artykuł dotyczy projektu innowacyjnej cewki do wytwarzania pól magnetycznych o indukcji ponad 55 T w objętości kilku dm<sup>3</sup>. W początkowej części opisana została budowa cewki. Użyteczne pole magnetyczne w tej cewce wytwarzane jest w cylindrycznej wnęce, umieszczonej mimośrodowo wewnątrz walca. Uzwojenie cewki składa się z przewodów, równoległych do osi walca i wnetki oraz przechodzących na zewnątrz tego układu. Przewody wykonane są z wolframu i chłodzone ciekłym helem. W następnej części wyznaczono rozkład przestrzenny indukcji wytwarzanego pola magnetycznego. Przeprowadzono obliczenia przybliżone dla cewki długiej oraz dokładniejsze obliczenia dla cewki o ograniczonej długości. Obliczono również podstawowe parametry układu zasilania i chłodzenia tej cewki. Porównano uzyskane wyniki z obecnymi możliwościami technicznymi i przedyskutowano wykonalność projektu. Istotnymi zaletami cewki są: duża jednorodność wytwarzanego pola magnetycznego, zredukowanie pola rozproszonego na zewnątrz oraz niewielka moc strat cieplnych.

*Słowa kluczowe:* cewka, walec, wnęka, pole magnetyczne, jednorodność, wolfram, chłodzenie, ciekły hel

